R66FPD284

INTERIM REPORT NO. 2

DISPERSION-STRENGTHENED CHROMIUM ALLOYS

by

R. E. Allen

Prepared for

NATIONAL AERONAUTICS AND SPACE ADMINISTRATION

OCTOBER 20, 1966

CONTRACT NAS 3-7607

NASA - Lewis Research Center
Cleveland, Ohio
John P. Merutka, Project Manager
Alan Arias, Project Advisor

GENERAL ELECTRIC COMPANY
Cincinnati, Ohio 45215

R66FPD284

DISPERSION-STRENGTHENED CHROMIUM ALLOYS

by

R. E. Allen

Prepared for

NATIONAL AERONAUTICS AND SPACE ADMINISTRATION

CONTRACT NAS 3-7607

MATERIALS DEVELOPMENT LABORATORY
ENGINEERING DEPARTMENT
GENERAL ELECTRIC COMPANY

TABLE OF CONTENTS

LIST OF FIGURES

LIST OF TABLES

1. ABSTRACT

Mechanical mixtures of submicron elemental powders of chromium, molybdenum and Y_2O_3 or MgO were densified by gas pressure bonding followed by extrusion. A Cr-5 $^{v}/o$ Y_2O_3-1Mo-0.15 each Hf, Th, Y alloy thus fabricated had an 800°F flow strength of 87 ksi and a ductile-to-brittle transition temperature of approximately 200°F. Cursory oxidation tests of this material in static air indicate that it compares favorably with the most oxidation resistant cast chromium alloys. Excess oxygen contamination in the densified alloy led to an order of magnitude increase in dispersoid particle size and interparticle spacing during a one hour vacuum exposure at 2600°F. In order to eliminate such growth, a cleaning technique for removal of interstitials was developed. This process is capable of reducing oxygen contamination in as-milled pure chromium powder to 130 ppm oxygen.

2. SUMMARY

1. The powder metallurgy process developed in this contract is capable of producing oxide dispersion strengthened Cr alloys with metallographic parameters which meet project goals of 1.5 micron interparticle spacing (IPS) and 0.1 micron particle size.

2. Interstitial contamination in the alloys produced, however, leads to severe dispersoid instability problems in which these parameters may increase by more than one order of magnitude during a one hour vacuum exposure at 2600°F.

3. The principle offender in oxide particle growth is oxygen. MgO or Y_2O_3 combine with Cr_2O_3 contamination present in the as-compacted alloy to form a double oxide (e.g., $YCrO_3$). This reaction leads to void formation, particle growth and an associated increase in interparticle spacing (IPS).

4. A carbothermic cleaning method has been developed which is capable of reducing oxygen contamination in the as-milled pure Cr powders to 130 ppm.

5. Cr-5 $^{v}/o$ Y_2O_3 powders were cleaned at 2200°F/20 min/vac and extruded at 2000°F. The resulting compact had an interparticle spacing (IPS) of 1.6 microns with an average dispersoid size of 0.07 micron.

6. This alloy has a flow stress of 87 ksi at 800°F and a ductile-to-brittle transition temperature of approximately 200°F. Inadequate powder handling after cleaning but prior to densification (autoclave

+ extrude) led to recontamination by oxygen and subsequent dispersoid instabilities in the above alloy. These instabilities, coupled with possible excess amounts of reactive element additions (REA) caused a hot short type of intergranular failure at very low stress (2.2 ksi) during a 2000°F tensile test.

3. INTRODUCTION

It was shown previously [1] that low temperature ball milling of mechanical mixtures of chromium, molybdenum and an oxide dispersoid produced powder size distributions which were 99% less than 0.5 microns. When compacted to full density by autoclaving plus extrusion this powder metallurgy product closely approached the microstructural parameter goals of 1.5 micron IPS and 0.1 micron particle size. The densified alloy contained excess interstitial elements, however, which led to considerable dispersoid instability. IPS and particle size increased by an order of magnitude, for example, during a 2600°F/1 hr thermal exposure of this material. Dispersoid growth was accompanied by other metallographic instabilities such as grain growth, recrystallization, and void formation. Since high temperature properties of dispersion strengthened materials are vitally dependent on a stable microstructure, dispersoid stability is a necessary requirement in the development of a successful high temperature alloy.

The application of chromium alloys to jet engine hardware demands the development of an alloy with usable low temperature ductility. The realization of this ductility goal in oxide dispersion strengthened chromium alloys may be accomplished by one of the several mechanisms proposed by Hahn and Rosenfield [2]. One mechanism, for example, is that second phase particles may partially deflect a crack after nucleation, thereby raising the energy for propagation. They also propose the possibility that glide dislocations nucleated at the particle under the influence of the stress field of the crack could effectively blunt the crack to prevent further propagation. The effect of grain size on ductility may also play an important role in fine grained dispersion strengthened alloys. Several BCC metals show decreasing ductile-to-brittle transition temperature (DBTT) with decreasing grain size [2]. There is conflicting evidence in the literature, however, as to the effect of grain size on ductile-to-brittle transition temperature (DBTT) in chromium (Figure 1). Cairns and Grant [3], for example, showed that DBTT increased with increasing grain size. This was in contradiction to the results of Gilbert [4]

and Allen [5] who showed that DBTT decreased with increasing grain size. This confusion is evidently the result of a difficulty in separating grain size effects from interstitial purity effects. The DBTT in chromium 30 [6] indicates that purity is probably governing the results of Gilbert [4] and Allen [5] since chromium 30 results fall in line with those of Cairns and Grant. Chromium 30 (Cr-MgO) with a grain size of approximately 25 microns had a 75°F DBTT despite relatively high interstitial contamination (0.7% excess oxygen) evidently as a result of the gettering ability of the MgO. This gettering action results in dispersoid coarsening and void formation.

If this reaction and accompanying void formation could be minimized by using high purity starting materials, and further, if particle size and IPS could be reduced by at least an order of magnitude, chromium 30 types of materials may be rendered ductile at room temperature and stable at high temperatures.

4. POWDER CLEANING INVESTIGATION

4.1 SOURCE OF CONTAMINATION

Alloys compacted to date have shown "tramp" interstitial contents in the range from 0.36 to 1.7%. This contamination originates from three main sources: i) powder production, ii) ball milling, and iii) powder handling. Elemental chromium powders purchased for this investigation were produced by magnesiothermic reduction of Cr_2O_3 and contain 0.5% oxygen and 0.08% carbon "as-purchased". The above oxygen contamination includes 0.25% MgO which is residual from the original reduction process.

In addition to the impurities inherited from powder production, additional impurities result from the -50°F ball milling treatment. Adsorption of carbon from ACS grade toluene grinding fluid onto freshly produced powder surfaces results in carbon contents as high as 0.7% after milling. The final carbon content of the powder is a function of ball milling time as is shown in Figure 3. Further oxygen contamination of the purchased powders during powder handling procedures has been very small although recent results indicate that after cleaning, the powders may be especially susceptible to oxygen contamination. This problem will be discussed in more detail in a later section.

4.2 CLEANING PROCESSES INVESTIGATED

Since the major interstitial contaminants were oxygen and carbon, the various cleaning investigations focused on them. Initially, cleaning was to be carried out with one element at a time. This approach proved to be unsuccessful, however, and the final investigation involved removal of both oxygen and carbon simultaneously.

4.2.1 Elimination of Carbon

Carbon contamination of these powders is especially critical since small amounts of carbon result in excessive quantities of carbide. In the compacted alloy, the volume percent of carbide is equal to 18.3 times weight percent of carbon. Powders with 0.6% carbon and 5 $^{v}/_{o}$ oxide could therefore conceivably contain 16 $^{v}/_{o}$ of a second phase after compaction.

Inefficient removal of toluene after ball milling was considered as a cause of contamination, but vacuum evaporation of the toluene in the temperature range from 200° to 300°F does not improve the efficiency of removal over that at room temperature. Replacement of toluene by another organic liquid was also considered and an attempt was made to displace the adsorbed toluene with a volatile liquid which could be more easily removed. The procedure used was as follows: as-milled dry powder was added to a flask of the liquid under investigation, shaken well, and allowed to settle. After decanting the liquid, the powders were dried at room temperature by vacuum evaporation. The effect of this procedure, used in conjunction with several different liquids, is reported in terms of powder carbon content in Table II.

4.2.2 Removal of Carbon and Oxygen

4.2.2.1 Hydrogen Cleaning - Both carbon and O_2 may be eliminated with a H_2 treatment carried out under the proper conditions. The reactions of interest here are:

$$C + 2H_2 \rightarrow CH_4 \qquad \text{(Equation 1)}$$

$$1/6\ Cr_{23}C_6 + 2H_2 \rightarrow 23/6\ Cr + CH_4 \qquad \text{(Equation 2)}$$

$$Cr_2O_3 + H_2 \rightarrow 2Cr + 3H_2O \qquad \text{(Equation 3)}$$

The operating conditions where the free energy of reaction is negative for Equations 1 and 2 are shown schematically in Figure 4. It may be seen here that Equation 2 requires very refined experimental procedures in terms of hydrogen purity. In the temperature region of interest (1000°-2000°F), for example, the $P_{CH_4}/P^2_{H_2}$ ratio must be less than 10^{-5} or 10^{-6} respectively in order for the free energy of reaction to be negative. Removal of carbon according to Equation 1, on the other hand, is much less demanding, especially in the range from 800° to 1200°F. In this range, the equilibrium $P_{CH_4}/P_{H_2} \gg 1$ and the reaction should progress quite readily in relatively impure hydrogen. The reduction of oxygen according to Equation 3 is well documented[8, 9] and may be accomplished in commercially pure cylinder hydrogen over a relatively wide range of temperatures. At 1800°F, for example, the reaction is feasible if the dew point is less than -40°F.

According to the above analysis, the first step of the cleaning process should be removal of adsorbed carbon at a low enough temperature to avoid carbide formation. The temperature could then be increased in the second step to implement the reduction of Cr_2O_3. The problem here is that the operating conditions which give de-oxidation may cause carburization of the powders if the hydrogen contains appreciable methane concentrations.

The hydrogen cleaning apparatus used in this study is shown schematically in Figure 2a. The powders, which were loaded into the stainless steel cleaning capsule in air, were subjected to alternate hydrogen flow (one hour) and vacuum (1/2 hour) cycles at 1800°F. A vacuum cycle was used in an effort to aid removal of the reaction products from the interstices between powder particles. Carbon content of powders subjected to this cleaning procedure is given in Table III.

As illustrated by the increase in carbon contents during cleaning runs 3, 4, and 5, the P_{CH_4}/P_{H_2} ratio was evidently too high in the hydrogen used. Whether this resulted from small amounts of impurities in the purchased (99.999% H_2) gas or from contamination in the gas train is not known. In any case, the powders were actually carburized during cleaning (starting carbon = 0.73%). In runs 1 and 2, the powders were decarburized, evidently as a result of inefficient exposure to hydrogen. In the first run, the powders were blown out of the capsule by excessive gas flow and the helium backfill after each vacuum cycle filled the voids with helium. Subsequent H_2 flow evidently did not cause an effective displacement of this helium by hydrogen. Powder from the second run was autoclaved after cleaning. Chemical analysis of the compact indicated that neither carbon nor oxygen were effectively reduced. Vacuum fusion analysis for gas content of this sample showed 2.040% O_2, 0.0078%N_2 and 0.0028%H_2 in addition to the 0.54% carbon. Powder handling procedures during compaction could have caused the oxygen contamination, but the lack of carbon removal was due to deficiencies in the cleaning process itself, as was later shown in runs 3, 4, and 5.

Since the elevated temperature exposure was necessary for removal of oxygen, and since no elaborate hydrogen purification apparatus was available for the required removal of carbon-bearing impurities from the cleaning gas, this technique was abandoned.

4.2.2.2 Carbothermic Cleaning - The second technique investigated utilizes the following reaction for interstitial cleaning:

$$3C + Cr_2O_3 \rightarrow 3CO + 2Cr \qquad \text{(Equation 4)}$$

The equilibrium between carbon, O_2 and chromium at elevated temperature and reduced pressure can be described in more detail through the use of the Pourbaix-Ellingham diagram[10] shown in Figure 5. The operating conditions corresponding to equilibrium between various two-phase combinations are appropriately labeled on the diagram; e.g., if temperature and pressure are regulated such that they lie above the upper line, the equilibrium phases will be Cr_2O_3 and carbon. All carbides are metastable in this region and would tend to decompose to graphite according to the reaction $Cr_xC_y + zO \rightarrow x/2\ Cr_2O_3 + yCO$. Likewise, if the operating conditions (P_{CO}, and temperature) are held in the region below the lower line, all Cr_2O_3 should be reduced according to Equation 4. The effective removal of both carbon and O_2 is therefore a matter of adjusting the operating conditions and the carbon content so that at the end of an isothermal cleaning treatment, the original chromium, carbon, Cr_2O_3 mixture has traversed the two phase fields from high P_{CO} to low P_{CO} and has arrived at the lower line with only trace amounts of Cr_2O_3 and $Cr_{23}C_6$ remaining.

Cleaning was carried out initially in a 1 1/2 inch ID, tantalum wound resistance furnace which was operated inside a vacuum (10^{-5} torr) glove box. All powder handling was carried out in this chamber. Loose, as-milled powders were spread out in a thin layer on metal trays and placed in the horizontal tube furnace for cleaning. These trays were made of either tantalum, zirconium, or titanium each of which is an excellent "getter" for interstitials. The experimental variables investigated were temperature, time, powder depth and tray (getter) material. Evaluation of the cleaning procedure was in terms of gas analysis of the loose powders. The powders were encapsulated

under helium in a small tin capsule which was transported to the vacuum fusion apparatus in a helium filled glass capsule where it was analyzed for oxygen, hydrogen and nitrogen. Carbon content of the powders was measured using air handling procedures in conjunction with either gravimetric or conductometric analysis.

Starting material for this series of experiments was a Cr-5 $^{v}/_{o}$ MgO-1.0Mo-0.25 Hf, Th, Y alloy which had been ball milled at -50°F for 500 hours in toluene. In addition to the 2.6% MgO which was added as dispersoid, the powder contained 0.25% MgO which was residual from the powder production process. Total oxygen content prior to cleaning was 1.04% as dispersoid, 0.10% (production MgO) and 0.46% as contamination. The results of this series of powder cleaning runs is given in Table IV (Numbers 10 thru 16). Oxygen content in this table is reported as the contamination portion of the total oxygen concentration and was derived by subtracting either 0.10% or 1.14% from the analyzed total oxygen content. The data tabulated in Numbers 10 thru 16 of Table IV is also shown graphically in Figures 6 and 7. Figure 6 demonstrates the effect of cleaning temperature on carbon content with time and "getter" materials as parameters. A comparison of the efficiency of gettering materials in aiding carbon removal made from this graph suggests that zirconium is the most efficient. Since zirconium has very poor high temperature strength, however, later experiments were conducted in tantalum boats with strips of zirconium sheet mixed in with the powder. Oxygen content of these same powders expressed as a function of cleaning temperature is given in Figure 7. Experimental difficulties inherent in analyzing a loose powder mixture containing an oxide dispersoid is evidenced by the large amount of scatter in these data. Credibility of the oxygen results was questioned still further when samples analyzed after densification by gas pressure bonding (Numbers 11 and 15 in Table IV) exhibited higher oxygen contents than did the loose powders. The higher oxygen content in the compacted alloy could have resulted from powder handling during densification, but the disagreement

could also be the result of dispersoid segregation or poor sampling of the loose powders. In an effort to resolve this difficulty, analytical techniques were unsuccessfully sought which would differentiate between MgO (Y_2O_3) and Cr_2O_3.

The above process was limited by the small furnace size to 5-20 gram sample sizes. In an effort to increase the output of the above furnace, an attempt was made to convert the cleaning from a batch process to a continuous process. Continuous cleaning was to be accomplished through use of a moving tray. Dwell time in the furnace hot zone was regulated by varying the speed of boat travel through the furnace. A line drawing of the apparatus used for the investigation of this continuous cleaning process is shown in Figure 2b. Initially, a fifteen inch long zirconium tray was moved slowly through the furnace hot zone (2200°F) with a dwell time of five minutes. Gas analysis of loose powders from this investigation indicated that neither carbon nor oxygen was being removed. This lack of cleaning was evidently the result of redeposition of both carbon and oxygen in cold portions of the furnace. A compromise between continuous and batch cleaning was then proposed in which several boats could be cleaned without breaking the vacuum. This semi-continuous method is identical to batch cleaning except several short boats were connected so that when one was in the hot zone, the others were completely outside the furnace. When cleaning of one tray was completed, a mechanical feed-through mechanism was actuated to pull it out of the furnace and simultaneously pull the next one into the hot zone. Chemical analysis of the powders cleaned using this procedure showed that while the powder from the second boat was cleaned (200 ppm carbon), powder from the first boat was not (1800 ppm carbon). This indicated that CO which was driven off the second boat was redeposited on the first despite that fact that it was outside the furnace. This phenomenon is further confirmed by consulting the Pourbaix-Ellingham diagram of

Figure 5 where the approximate operating conditions in the hot zone and in the colder portions of the furnace are noted. Equilibrium phases in the hot zone are $Cr_{23}C_7$ and chromium, while those in the cold zone are Cr_2O_3 and carbon. Carbon monoxide therefore transports carbon and oxygen from the center to the cold portions of the furnace, and only a small amount of cleaning is accomplished. All subsequent cleaning was therefore done by a batch process.

Powder processing reported thus far was carried out in three systems. Ball mill loading was done in an argon filled non-vacuum glove box, cleaning in a vacuum glove box which had no airlock, and final sealing of the encapsulated powders was accomplished in an EB welding chamber. The inefficiencies inherent in the use of three separate facilities was therefore greatly improved by the installation of a glove box and airlock extension to the vacuum chamber of the EB welder. This equipment allowed all of the above operations to be carried out in one chamber, thereby reducing possibility of powder contamination during transfer from one system to another. All cleaning investigations reported in the following were carried out in this system which was equipped with a 2 1/2 inch ID, tantalum wound resistance furnace.

One hundred gram quantities of powder which were cleaned in preparation for extrusion were exposed for cleaning in a stack of three 2-inch X 5-inch tantalum boats with a 0.275-inch powder depth. A series of Cr 5 ^{v}/o Y_2O_3 alloys with 0.15, 0.25, and 0.35% each of Hf, Th, Y were cleaned in this fashion at 2200°F/20 min. In all three alloys the carbon content was reduced to approximately 60 ppm. Oxygen level of the loose powder was not monitored. As with the Cr + MgO powders, gas analysis after compaction indicates high oxygen content.

Foregoing results, obtained from chemical analysis of loose powders, indicate that both carbon and oxygen may be substantially reduced by carbothermic cleaning. Although analysis of loose powders indicated that the oxygen content was quite low, the data contained large amounts of scatter. High oxygen content of these same powders after compaction therefore raised a question as to the efficiency of the process in reducing oxygen. In order to answer this question, carbothermic cleaning was carried out on chromium powders which contained no oxide dispersoids. Analytical errors resulting from poor sampling of oxide dispersoids which were present in the powders were thereby eliminated. This work which is not fully completed is also reported in Table IV (1-5). Starting material was M&R chromium powder which was ball milled without dispersoid for 456 hours at -50°F in toluene. Carbon content of the as-milled powder was exceptionally low with the result that an insufficient quantity was available for stoiciometric combination with the 0.403% oxygen present as contamination. The analyses indicate that after a very rapid decarburization period, the powder was actually oxidized. The extent of this oxidation increased with increasing temperature. Carbon content of the cleaned powders was very low in those cases where the powder was cleaned at temperatures greater than 1800°F. Initial oxygen analysis indicated that oxygen was substantially reduced at 1600°F. Carbon analysis of the sample cleaned at 1600°F indicated only a small reduction of carbon thereby challenging the oxygen analysis. A recheck using powders which had been exposed to air showed only a minor reduction in oxygen which was in close agreement with the corresponding decrease of carbon. Powder cleaning reported in Table IV as Numbers 6 thru 9 was conducted using the same starting powders with an addition of high purity graphite. These results are also shown graphically in Figure 7 where they are compared with the results of the previously cleaned Cr + MgO powder. As shown, a 2400°F/50 min exposure of chromium graphite mixtures reduced the oxygen content to 130 ppm. Although the previous work with Cr + MgO indicates

complete removal of oxygen at a lower temperature than 2400°F in the same fifty minute exposure period, these results were obtained with powder depths of 0.05 inches as compared to a depth of 0.275 inches for the chromium-graphite mixture. Gas analysis of powders cleaned at 2400°F and subsequently exposed to air indicate that the product has sintered sufficiently that oxygen contamination from air handling was no longer a critical problem.

5. DISPERSOID STABILITY

As reported previously [1], the powder process developed in this investigation is capable of producing dispersion strengthened materials with the desired microstructural parameters. The MgO and Y_2O_3 dispersoids used here, however, were found to be unstable and underwent extensive growth during thermal exposure after compaction. The effects of the various vacuum heat treatments on microstructural parameters is shown in Table V. This data was generated using lineal analysis and the Zeiss TGZ-3 particle size analyzer. The dispersoid growth phenomenon is shown in more detail in Figure 8 which shows oxide particle size distributions after exposure to stability anneals in the temperature range 2000-26000°F. The particle size distribution after 2000°F exposure, shows a single peak at approximately 0.2 micron. In the sample exposed at 2600°F, however, there are now two peaks in the particle size distribution curve. The height of the peak at small particle size is decreasing while the number of particles found in the peak at 1.2 microns is increasing. This is a result of the growth of large particles at the expense of the smaller ones, i.e., particles above some average particle size d_o increase in diameter while particles less than d_o decrease in diameter with increasing time. Dispersoid instability is further evidenced by void formation and an accompanying decrease in bulk density of the alloy [1]. When exposed isothermally, a Cr-Y_2O_3 alloy with 0.15% REA showed very rapid particle growth initially which asymtotically approached some upper particle size. X-ray diffraction of extractions from Cr-5 $^{v}/_{o}$ Y_2O_3-1Mo-0.25% REA alloy as-compacted indicates the oxides were present as Y_2O_3, ThO_2 and Cr_2O_3. After a 2600°F/1 hr/vac stability anneal, the oxides were present almost entirely as $YCrO_3$. Photomicrographs showing the microstructure of this alloy before and after thermal exposure are presented in Figure 9. The extremely coarse $YCrO_3$ chromate particles shown in the lower photograph indicate that these oxides are polycrystalline. In addition, contact angles at triple point grain boundaries indicate that the interfacial energy between the $YCrO_3$ and the chromium is of the same order of magnitude

as the chromium grain boundary energies. This low energy, of course, would be very beneficial in preventing decohesion between particle and matrix upon application of stress. The results of a thermal stability anneal on a Cr-5 $^{v}/o$-Y_2O_3 alloy with 0% REA are shown in Figure 12. The microstructures of this alloy after a 2600°F/1 hr/vac. thermal exposure show considerable instability. It is obvious from these results that the reactive element additions do not act as catalytic agents in the dispersoid instability.

The effect of powder cleaning on metallographic parameters may be seen in Figures 10 and 11. These Cr-5 $^{v}/o$ MgO samples were cleaned according to the conditions shown in the figure and indicate that increasing time and temperature cause an increase in particle size. In each case, however, the final compact is high in oxygen either as a result of poor cleaning or as a result of recontamination during compaction. This effect may be the over-riding factor and may govern the growth shown in each case.

The possibility of eliminating glove box powder handling procedures prior to the powder cleaning step was investigated using elemental powders without REA or dispersoid. The ball mills were loaded and unloaded in the air and the milling was carried out in the standard manner at -50°F using toluene with an argon cover. Toluene was removed in air in a drying oven at approximately 200°F. Vacuum fusion analysis of this powder indicated that the air handling procedure prior to ball milling and prior to powder cleaning does not increase oxygen and therefore it seems possible that glove box handling could be at least partially eliminated. However, ordinary powder handling would increase health hazards from air-borne submicron metal powders and this elimination of inert handling procedures therefore seems unwise. In addition to these results on the effect of powder handling on contamination, the results of powder cleaning at temperatures less than 2200°F seem to indicate that this process makes the material extremely vulnerable to oxygen contamination during subsequent handling. This may necessitate an additional step to the cleaning process in which the powder would be heated

to 2600°F for fifteen minutes prior to cooling from the cleaning temperature. This would cause sintering of the powders and would decrease the surface area to such an extent that surface contamination would no longer be a problem. Powder cleaning carried out at 2400°F for thirty and fifty minutes, for example, indicate that the powder has sintered sufficiently even under these conditions that the subsequent air handling does not cause recontamination by oxygen.

6. EVALUATION OF REACTIVE ELEMENT ADDITIONS (REA)

Alloys with 5 $^{V}/o$ MgO and 5 $^{V}/o$ Y_2O_3 each with three different levels of REA were prepared by ball milling at -50°F for 500 hours in toluene. These alloys were cleaned by the carbothermic process at 2200°F for twenty minutes using a zirconium getter. Interstitial content of the compacted powders is shown in Table V. After autoclaving at 2000°F the Cr 5 $^{V}/o$ Y_2O_3 alloys were extruded at the General Electric Research and Development Center, Schenectady, New York, at 2000°F using a ratio of 14/1. The alloys which contained 0.15 and 0.25% REA extruded successfully and were evaluated in greater detail. The 0.3% REA alloy, on the other hand, extruded in many short segments which were not usable for detailed analysis of DBTT and tensile properties. Tensile tests were conducted on both of the sound alloys at ambient temperature and at 2000°F in vacuum. The button-head specimens used in the various tests are pictured in Figure 13.

As a result of the extensive surface irregularities in the extrusion, only three tensile specimens were obtained from the 0.15 REA alloy and two from the 0.25 REA alloy. Two of the 0.15 REA alloy samples were used in ductile-to-brittle transition tests (DBTT) and the third was tested in tension at 2000°F. DBTT was investigated using slow strain rate (0.5%/min) tensile loading to 1% plastic strain. After 1% plastic strain, the load was released, the temperature reduced 100°F, and the sample was again loaded to 1% strain. This procedure was repeated at 100°F increments until failure occurred. In the as-extruded alloy the test was initiated at 800°F and fracture occurred at 600°F. A very severe surface defect in the gage length, however, undoubtedly caused premature failure. The second sample was heat treated at 2000°F for one hour in vacuum prior to testing. A summary of the DBTT test of the second sample is shown in Figure 14 which is a reproduction of the Instron load versus extension chart. The test was initiated at 600°F where the flow stress was 87 ksi. Fracture occurred at room temperature after a total plastic strain of 5% resulting from five increments of 1% strain each.

Flow stress of these two alloys was approximately 100 ksi at ambient temperature and approximately 90 ksi at 800°F. A comparison to cast alloys with compositions comparable to that of the matrix indicates that dispersion strengthening contributed approximately 40 ksi to the fracture strength in this temperature range. At 2000°F both the 0.15 and the 0.25 REA alloys were extremely weak. Intergranular fracture occurred at 2.2 ksi for the 0.15% REA alloy and 5.7 ksi for the 0.25% REA alloy. Both alloys showed considerable ductility (45% and 26% elongation respectively) but contained many transverse intergranular surface cracks as shown in Figure 13. Such behavior is typical of hot shortness phenomenon experienced in previous chromium alloys as a result of excessive REA concentration[11]. This behavior is further magnified by the fact that extrusion does not produce a fibered structure which would minimize the effect of weak boundaries.

Oxidation tests at 2000°, 2400°, and 2600°F in static air compared very favorably with the most oxidation resistant cast chromium alloys and the results are summarized in Table VI. The oxide scale on these samples is quite adherent and nitride layers are not detectable metallographically.

7. DISCUSSION AND RECOMMENDATIONS

Since chromium has a DBTT which is strongly dependent upon interstitial content, it seems absolutely necessary that the oxide dispersoids be capable of gettering such impurities. The presence of oxygen as Cr_2O_3, for example, would seem to present an intolerable situation and even an excellent dispersion of a highly inert dispersoid such as ThO_2 would be fracture limited as a result of the excess oxygen in equilibrium with the chromium oxide. On the other hand, gettering type oxides are subject to thermal coarsening as a result of their scavenging action. The MgO in Cr-30 displays such behavior with the result that after a ductilizing anneal, dispersoid particle size is approximately 2-3 microns and IPS is approximately 25-30 microns. These parameters are at least an order of magnitude too large to bring about effective high temperature strengthening and microstructural stability. In order to avoid such extensive coarsening of the original microstructural parameters, it is necessary to start with purified powders which contain relatively low amounts of interstitial impurities. After compaction, this material would be exposed to a high temperature ductilizing anneal which would cause the reaction $MgO + Cr_2O_3$ to go to the $MgCrO_4$. Since the interstitial content of the starting materials would be very low, this reaction would be minimized and void formation reduced. After this limited amount of gettering was completed, growth of the dispersoid would occur only as Ostwald ripening. Dispersoid particle size would be expected to be extremely stable as a result of the high stability of this spinel coupled with the fact that the interfacial energy (driving force for growth) between chromium and the spinel is of the same order of magnitude as the chromium grain boundary energies.

An oxide dispersion strengthened chromium alloy with gettering capabilities but high interstitial content or an alloy with good stability but no gettering ability are both undesirable end products. The first alloy would have good low temperature ductility after gettering, but poor high

temperature strength as the result of the microstructural instabilities of dispersoid growth, void formation, and recrystallization. The alloy with good dispersoid stability should have excellent resistance to flow at high temperatures, but would be extremely notch-sensitive at low and intermediate temperatures as a result of the high interstitial content. The TD-nichrome analog in which two different dispersions coexist independently does not apply here, since chromium oxide is not extremely damaging to the nickel matrix in TD-nichrome, whereas such high interstitial contents in chromium would seem to be completely unacceptable.

The carbothermic cleaning process described previously should provide the critical step necessary for production of dispersion-strengthened chromium alloys in which a stable oxide dispersoid may be maintained after an initial gettering action. It seems likely that both cleaning and gettering will slightly degrade the metallographic parameters achieved in the as-milled powder blend, but improved dispersoid stability should compensate this loss.

REFERENCES

1. R. E. Allen and R. G. Carlson, Semi-Annual Report No. 1, NASA Contract NAS 3-7607 (December 1965).

2. G. T. Hahn and A. R. Rosenfield, TR AFML-TR-65-409 (January 1966).

3. R. E. Cairns and N. J. Grant, Trans AIME, 230, 1150 (1964).

4. A. Gilbert, C. N. Reid, and G. T. Hahn, J. Inst. Met., 92, 351 (1964).

5. B. C. Allen, D. J. Maykuth, and R. I. Jaffee, Trans AIME, 227, 724, (1963).

6. C. R. Manning, Jr., and D. M. Royster, NASA TN D-1785 (June 1963).

7. H. A. Johanson, H. L. Gilbert, R. G. Nelson, and R. L. Carpenter, U. S. Bureau of Mines Report on Investigation, 5058, (May 1954).

8. W. H. Chang, Welding Research Supplement, 622 (December 1966).

9. L. S. Darken and R. W. Gurry, Physical Chemistry of Metals, McGraw-Hill Book Company, Incorporated, New York (1953).

10. W. L. Worrell, Trans AIME, 233, No. 6, 1173 (1965).

11. J. W. Clark, First Semi-Annual Report, NASA Contract NAS 3-7260, (October 1965).

TABLE I

ELECTRON METALLOGRAPHIC PROCEDURES USED IN PREPARING SAMPLES

FOR QUANTITATIVE METALLOGRAPHY

No.	Polishing Procedure	Etchant	Replica
1	Etch-polish (syntron)	Kromic (electrolytic)*	2 stage C - Ge shadow
2	Electropolish	HCl/glycerine	2 stage C - Ge shadow
3	Hand polish - short nap - diamond and Linde B	HCl/glycerine	2 stage C - Ge shadow
4	Hand polish - short nap - diamond and Linde B	HCl/glycerine (Heavy etch)	Extraction replica

* Kromic Etching Solution - 100 ml. H_2O_2, 50 ml. KOH, 50 g. $K_3Fe(CN)_6$, 5 g. $K_4FE(CN)_6 \cdot 3H_2O$, 40 ml. H_3PO_4, 20 g. $H_2C_2O_4$, 5 - 10 volts, 2 - 3 amps/cm^2.

TABLE II

CARBON CONTENT OF AS-MILLED M&R Cr POWDERS AFTER APPLICATION OF VARIOUS TOLUENE DISPLACEMENT SOLVENTS

Solvent	ppm C
Trichloroethylene	5700
Xylene	6100
Benzene	6000
Hexane	7800
Ethyl Alcohol	6200
Acetone	6100

TABLE III

CARBON CONTENT OF M&R Cr POWDERS AFTER HYDROGEN CLEANING*

Run No.	Environment	Temp °F	No of Cycles (1 hr H_2+1/2 hr vac)	% C Final	Remarks
1	H_2 (99.92%)	1800	9	0.034	Powder blown out of SS capsule
2	H_2 (99.999%)	1800	9	0.54	Capsule backfilled each cycle with He before starting H_2 flow
3	H_2 (99.999%)	1800	4	1.04	No He used- capsule backfilled directly with H_2
4	H_2 (99.999%)	1800	3 hr H_2 + 2 cycles	1.34	Thin layer of powder on Mo tray
5	H_2 (99.92%)	1800	4 hr H_2	1.92	Thin layer of powder on Mo tray

* Starting powder - M&R Cr-2.8 Mo-5 v/o MgO-0.25 each Hf, Th, Y. Ball milled 500 hrs/-50°F/toluene (7300 ppm C).

TABLE IV

GAS ANALYSIS OF LOOSE Cr POWDERS AFTER CARBOTHERMIC CLEANING

No	Powder	Cleaning Conditions (temp °F/time min/powder depth/type getter)	C		O(1)	
			Initial	Final	Initial	Final
1	As-milled M&R Cr	2070/50/.05/Zr	0.124	0.006	0.4030	0.555
2	As-milled M&R Cr	2070/5/.275/Zr	0.124	0.006	0.4030	0.557
3	As-milled M&R Cr	2350/50/.275/Zr	0.124	0.007	0.4030	0.637
4	As-milled M&R Cr	1800/10/.275/Zr	0.124	0.008	0.4030	0.477
5	As-milled M&R Cr	1600/10/.275/Zr	0.150	0.131	0.6750	0.2610? 0.6520
6.	As-milled (Cr+graphite)	1800/5/.275/Zr	0.5750	0.5520	0.580	0.697
7.	As-milled (Cr+graphite)	2070/5/.275/Zr	0.5750	0.3250	0.580	0.424
8.	As-milled (Cr+graphite)	2400/33/.275/Zr	0.6150	0.1460	0.6080	0.2125
9.	As-milled (Cr+graphite)	2400/50/.275/Zr	0.6150	0.0645	0.608	0.0130
10.	As-milled (Cr+5 V/o MgO+ 0.25 each Y,Th,Hf)	2000/5/.05/Ta	0.570	0.0600	0.460	0.670
11.	As-milled (Cr+MgO+Y,Th,Hf) (same as No. 10)	2200/5/.05/Ta	0.570	0.0445	0.460	0.10 0.47(2)
12.	As-milled (Cr+MgO+Y,Th,Hf)	2400/5/.05/Ta	0.570	0.0360	0.460	0.40(2)
13.	As-milled (Cr+MgO+Y,Th,Hf)	2400/5/.275/Ta	0.570	0.0950	0.460	0.36
14.	As-milled (Cr+MgO+Y,Th,Hf)	2100/50/.05/Ti	0.570	0.0425	0.460	-0.006(3)
15.	As-milled (Cr+MgO+Y,Th,Hf)	2000/50/.05/Zr	0.570	0.0160	0.460	-0.022 0.32(2)
16.	As-milled (Cr+MgO+Y,Th,Hf)	2400/50/.05/Zr	0.570	0.0205	0.460	-0.48
17.	As-milled (Cr+MgO+Y,Th,Hf)	2000/50/.05/Ta	0.570	0.0140	0.460	-

(1) Oxygen is reported as that which is not combined with MgO. (As-purchased M&R Cr powders contain 0.25% MgO.)

(2) After compaction by autoclaving at 2000°F/2 hrs/10 ksi He.

(3) Negative sign indicates total oxygen by chemical analysis is less than oxygen added as MgO.

TABLE V

QUANTITATIVE METALLOGRAPHIC PARAMETERS OF COMPACTED Cr ALLOYS

Sample	Autoclave (°F/hours/ksi)	Extrusion (°F/ratio)	Vacuum Heat Treat (°F/hours)	Dispersoid (5 v/o)/% REA	% Mo	% C	% O (excess)	ppm H	ppm N	IPS (μ)/magnification	Particle Size (Avg Intercept)/ Magnification	v/o Dispersoid (added)	v/o Dispersoid (measured)
472	2000/2/10	-	-	MgO/.25	3.9	.230	0.5	41	45	$3.4/10^4$	$0.39/10^4$	5	10.3
472	2000/2/10	-	2000/1	MgO/.25	3.9	-	-	-	-	$5.9/10^3$	$0.58/10^3$	5	9.9
472	2000/2/10	-	2200/1	MgO/.25	3.9	-	-	-	-	$6.7/10^3$	$0.50/10^3$	5	7.4
472	2000/2/10	-	2400/1	MgO/.25	3.9	-	-	-	-	$10.4/10^3$	$0.52/10^3$	5	5.0
472	2000/2/10	-	2600/1	MgO/.25	3.9	-	-	-	-	$10.8/10^3$	$1.08/10^3$	5	10.0
As-Recd Cr+MgO	2000/2/10	-	-	MgO/0	0	.080	0.5	-	50	$24.6/10^3$	$1.2/10^3$	5	-
As-Recd Cr+MgO	2000/2/10	-	2400/1	MgO/0	-	-	-	-	-	$25.3/10^3$	$1.2/10^3$	5	-
As-Recd Cr+MgO	2000/2/10	-	2600/1	MgO/0	-	-	-	-	-	$23.8/10^3$	$1.2/10^3$	5	-
As-Recd Cr+Y_2O_3	2000/2/10	-	-	MgO/0	0	.080	0.5	-	50	$25.3/10^3$	$1.15/10^3$	5	4.8
As-Recd Cr+Y_2O_3	2000/2/10	-	2400/1	MgO/0	-	-	-	-	-	$25.1/10^3$	$0.97/10^3$	5	3.7
As-Recd Cr+Y_2O_3	2000/2/10	-	2600/1	MgO/0	-	-	-	-	-	$25.0/10^3$	$1.37/10^3$	5	5.3
463	2000/2/8	-	-	MgO/.25	23	.650	0.10	40	120	$.8/10^4$	$0.05/10^4$	5	5.9
463	2000/2/8	-	-	MgO/.25	23	.650	0.10	40	120	$4/10^3$	$0.34/10^3$	5	5.9
463	2000/2/8	-	2000/1	MgO/.25	23	-	-	-	-	$5.2/10^3$	$0.33/10^3$	5	6.0
463	2000/2/8	-	2200/1	MgO/.25	23	-	-	-	-	$5.5/10^3$	$0.35/10^3$	5	8.2
463	2000/2/8	-	2400/1	MgO/.25	23	-	-	-	-	$4.3/10^3$	$0.36/10^3$	5	4.4
463	2000/2/8	-	2600/1	MgO/.25	23	-	-	-	-	$10.0/10^3$	$0.46/10^3$	5	7.8
110.5A	1900/3/10	-	-	MgO/.25	3.6	.140	1.0	1	38	$1.9/10^4$	$0.22/10^4$	5	10.4
110.5A	1900/3/10	-	2200/100	MgO/.25	-	-	-	-	-	$3.65/10^3$	$0.80/10^3$	5	18.3
2-463	1900/2/10	-	-	MgO/.25	23	.670	0.5	18	110	$2.45/10^3$	$0.36/10^3$	5	13.0
2-463	1900/2/10	-	2000/1	MgO/.25	23	-	-	-	-	$8.6/10^3$	$0.25/10^3$	5	2.9
2-463	1900/2/10	-	2200/1	MgO/.25	23	-	-	-	-	$10.8/10^3$	$0.27/10^3$	5	2.5
2-463	1900/2/10	-	2400/1	MgO/.25	23	-	-	-	-	$5.3/10^3$	$0.34/10^3$	5	5.9
2-463	1900/2/10	-	2600/1	MgO/.25	23	-	-	-	-	$9.6/10^3$	$0.67/10^3$	5	6.5
500-1A cleaned 2000°/5 min/vac	2000/2/10	-	-	MgO/.25	1.0	.060	0.65	21	49	$3.4/10^4$	$0.41/10^4$	5	11.9
500-1A cleaned 2000°/50 min/vac	2000/2/10	-	-	MgO/.25	1.0	.042	0.32	252	-	$4.0/10^4$	$0.46/10^4$	5	11.3
500-5A	2400/2/10	-	-	MgO/.25	5.98	.680	1.0	41	90	$11.0/10^3$	$1.26/10^3$	5	10.2
500-5A	2400/2/10	-	1800/1	MgO/.25	-	-	-	-	-	$9.2/10^3$	$1.20/10^3$	5	11.4
500-5A	2400/2/10	-	2000/1	MgO/.25	-	-	-	-	-	-	-	5	-
500-5A	2400/2/10	-	2200/1	MgO/.25	-	-	-	-	-	-	-	5	-
500-5A	2400/2/10	-	2400/1	MgO/.25	-	-	-	-	-	$10.9/10^3$	$1.48/10^3$	5	10.9
2200/20 min/clean	2000/45 min/5	-	-	Y_2O_3/.15	0.9	.0060	0.79	59	29	$1.6/10^4$	$0.07/10^4$[1] $0.28/10^4$	5	15.3
2200/20 min/clean	2000/45 min/5	1000/14/1	2400/100/air	Y_2O_3/.15	-	-	-	-	-	$12.0/10^3$	$1.40/10^3$	5	10.6
2200/20 min/clean	2000/45 min/5	1000/14/1	2400/10/air	Y_2O_3/.15	-	-	-	-	-	$12.2/10^3$	$1.80/10^3$	5	12.6
1800/5 min/clean	1800/10 min/ hot press	-	-	Y_2O_3/0	3.45	.0160	1.26	82	31	$4.1/10^3$	-	5	-
1800/5 min/clean	1800/10 min/ hot press	-	2600/1	Y_2O_3/0	-	-	-	-	-	$12.0/10^3$	-	5	-

(1) Particle size determined on an extraction replica.

TABLE VI

OXIDATION RESULTS OF Cr-5 $^{V}/_{O}$ Y_2O_3-1.0Mo-.15 ea Hf, Th, Y

Heat	Temp (°F)	Time (hrs)	Avg. Weight Change (mg/cm^2)
1	2000	10	+ 2.21
2	2000	100	- 3.53
3	2400	10	+ 2.36
4	2400	100	- 9.45
5	2600	10	+ 109.0

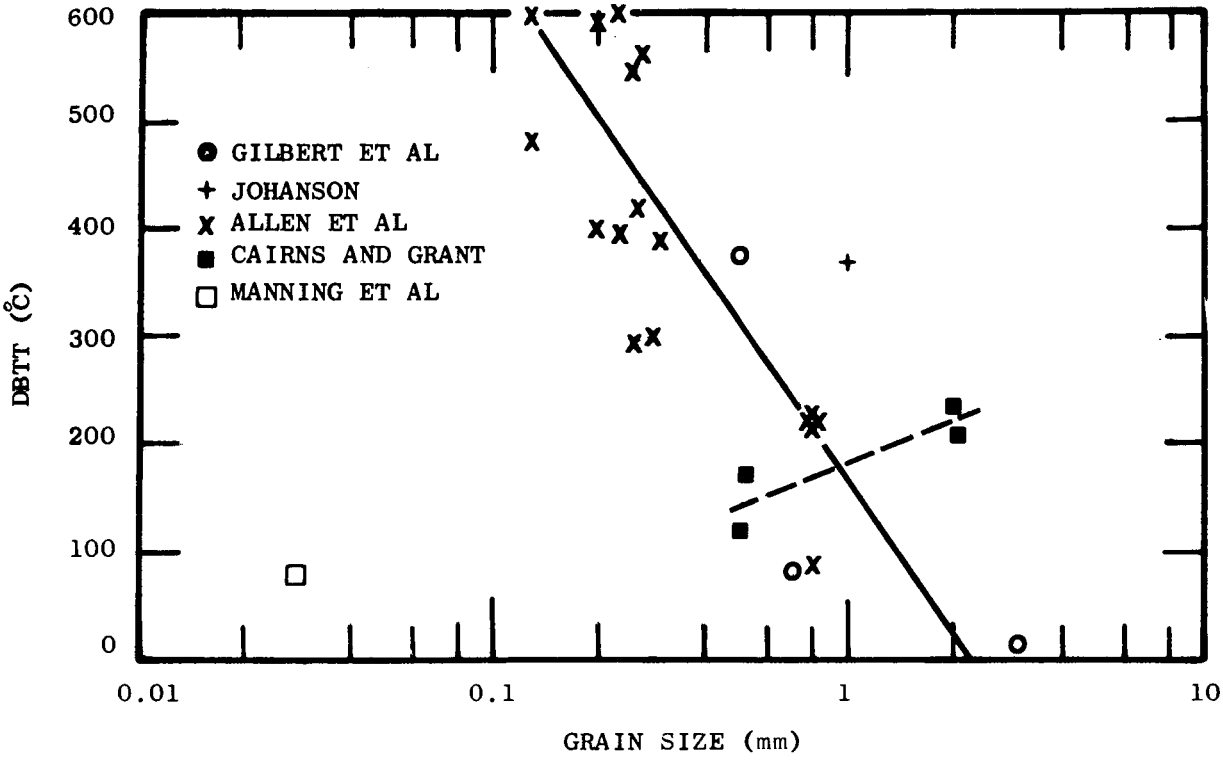

FIGURE 1 Effect of Grain Size on Transition Temperature of Cr [a].

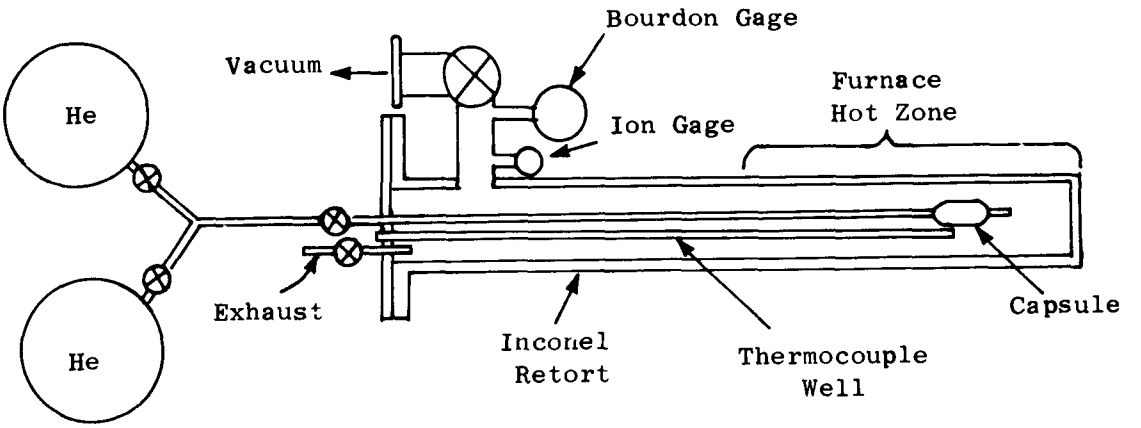

(a)

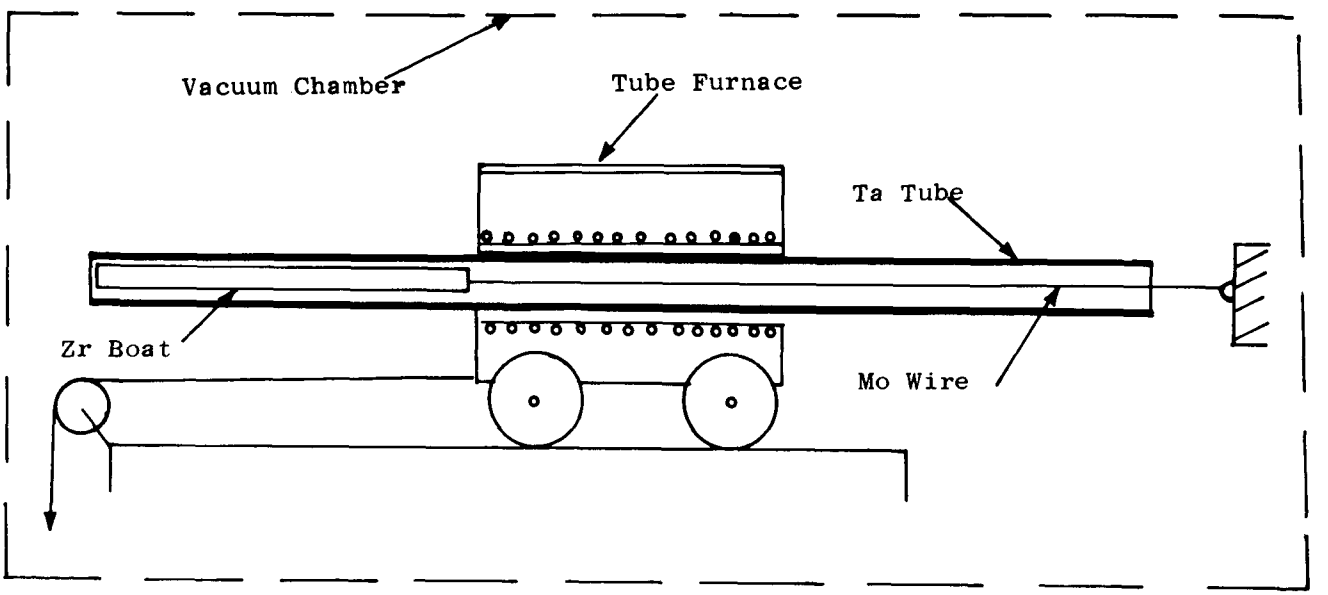

(b)

FIGURE 2 Schematic Diagrams of Experimental Equipment Used for: (a) H_2 Cleaning, and (b) Continuous Carbothermic Cleaning.

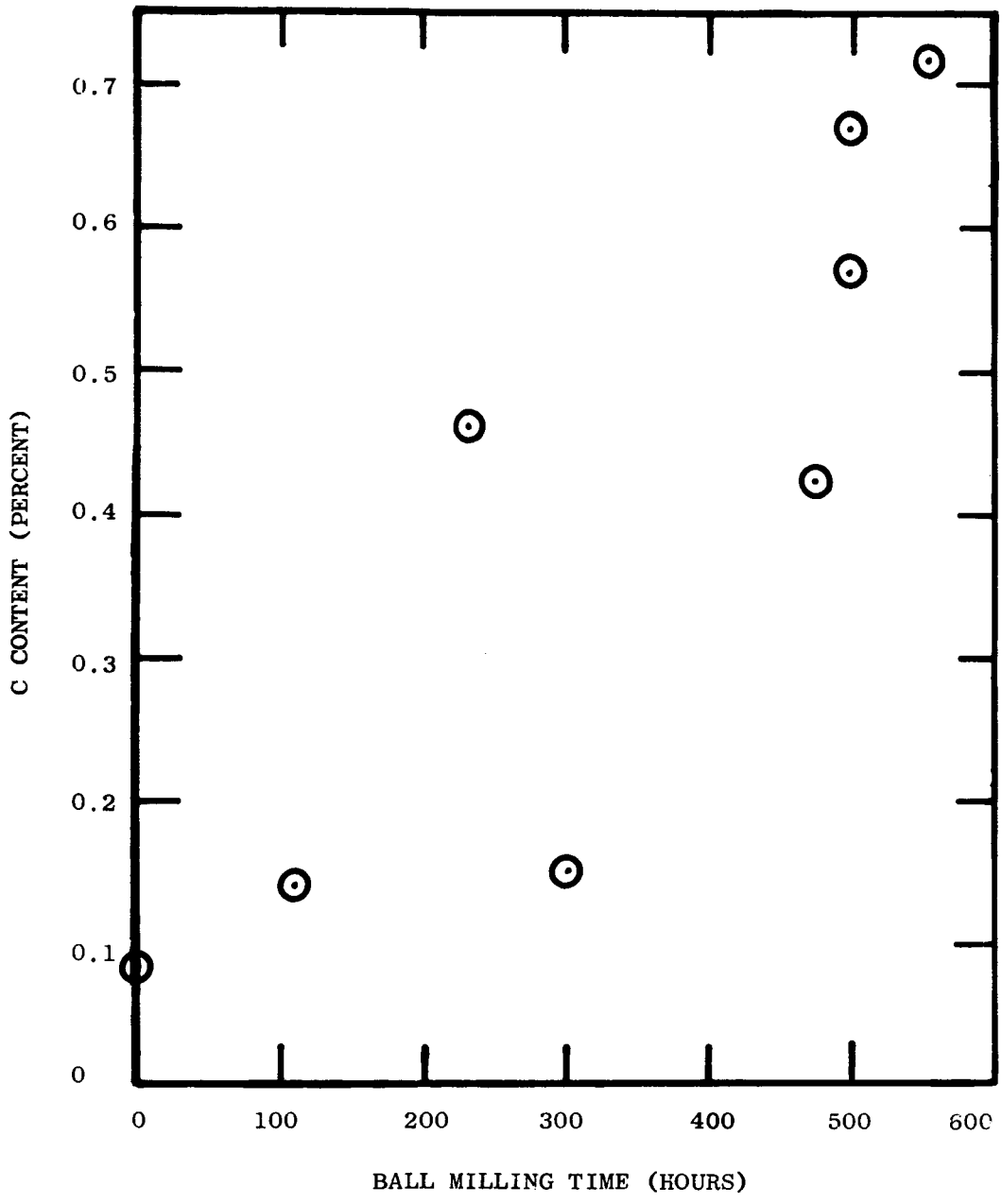

FIGURE 3 Carbon Content of Elemental Cr Powders + Oxide Dispersoid As a Function of Ball Milling Time.

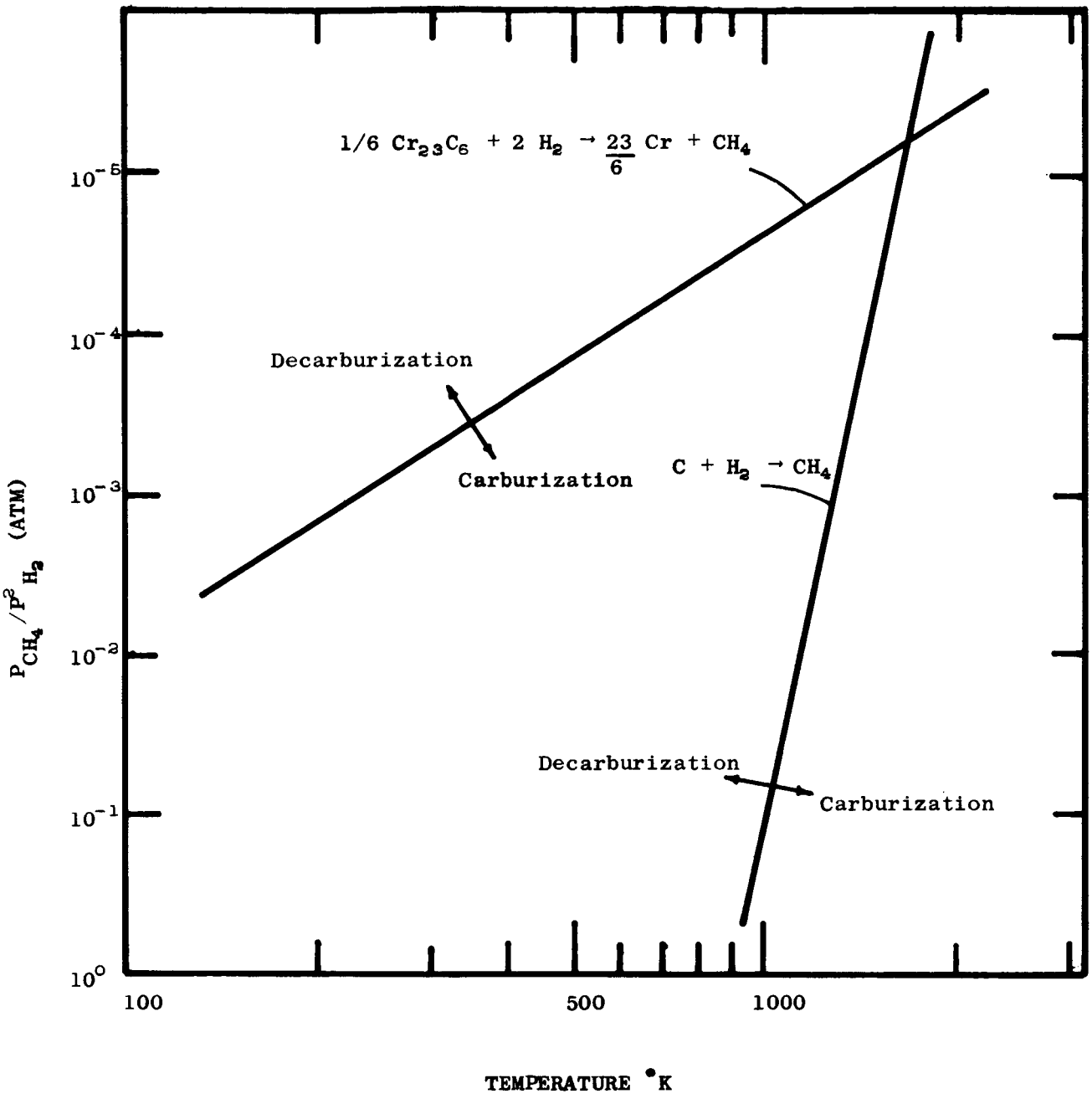

FIGURE 4 Ratio of $P_{CH_4}/P^2_{H_2}$ Necessary for H_2 Removal of Carbon from Cr As a Function of Temperature.

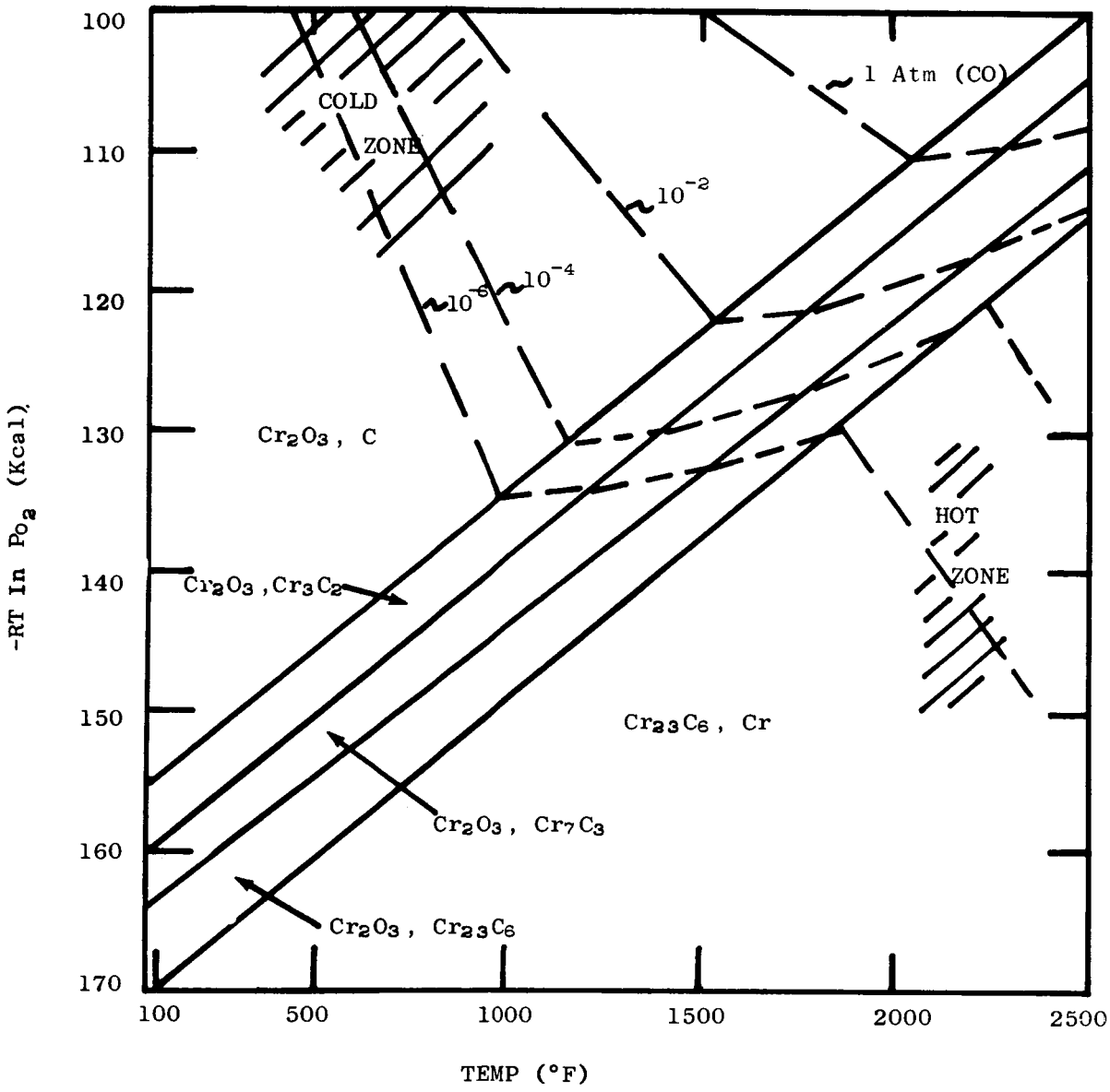

FIGURE 5 Pourbaix-Ellingham Diagram for the Cr-C-O System.

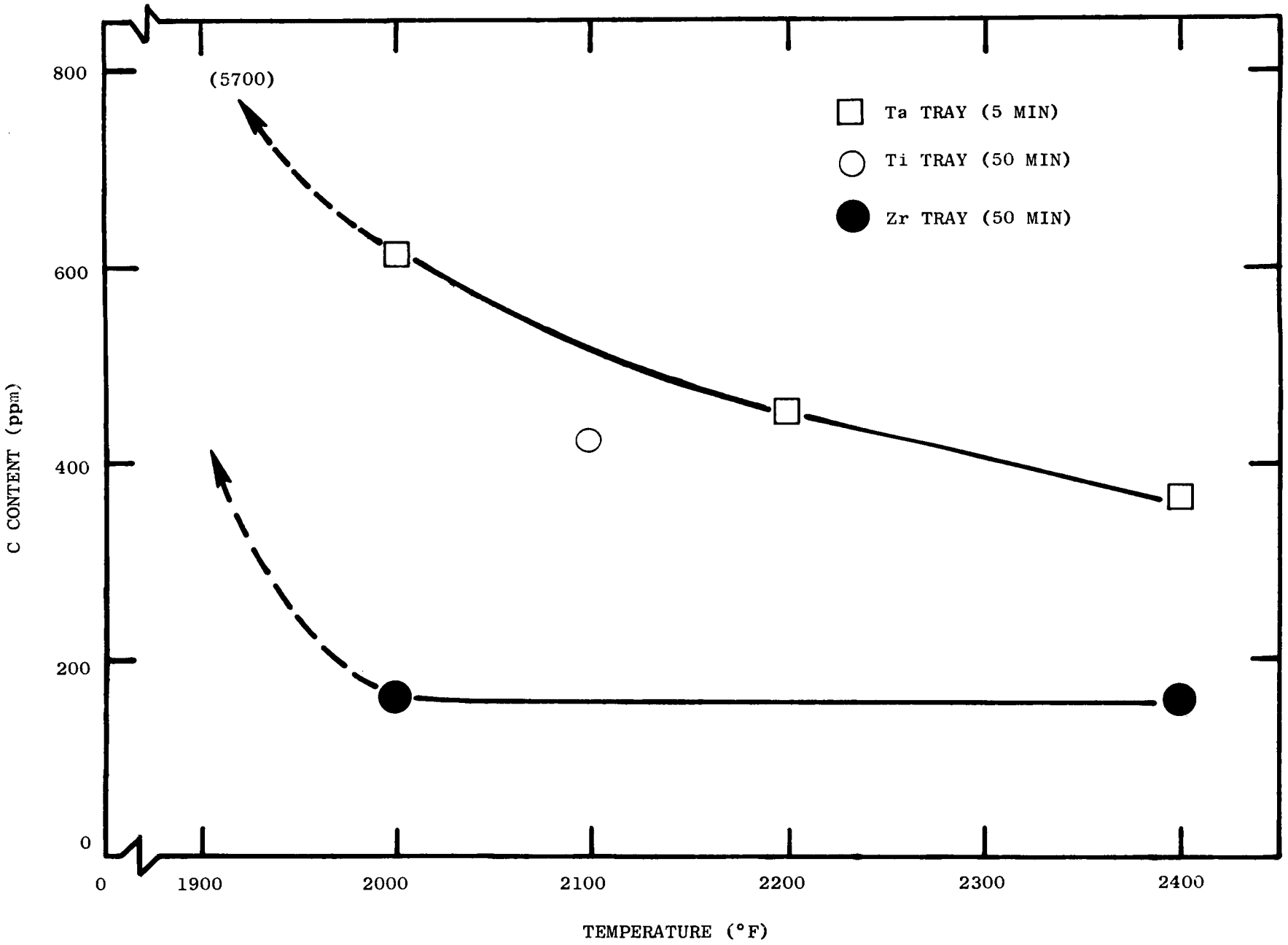

FIGURE 6 Carbon Content as a Function of Temperature for Carbothermic Cleaning of M&R Cr Powders Containing 5 $^{V}/_{o}$ MgO.

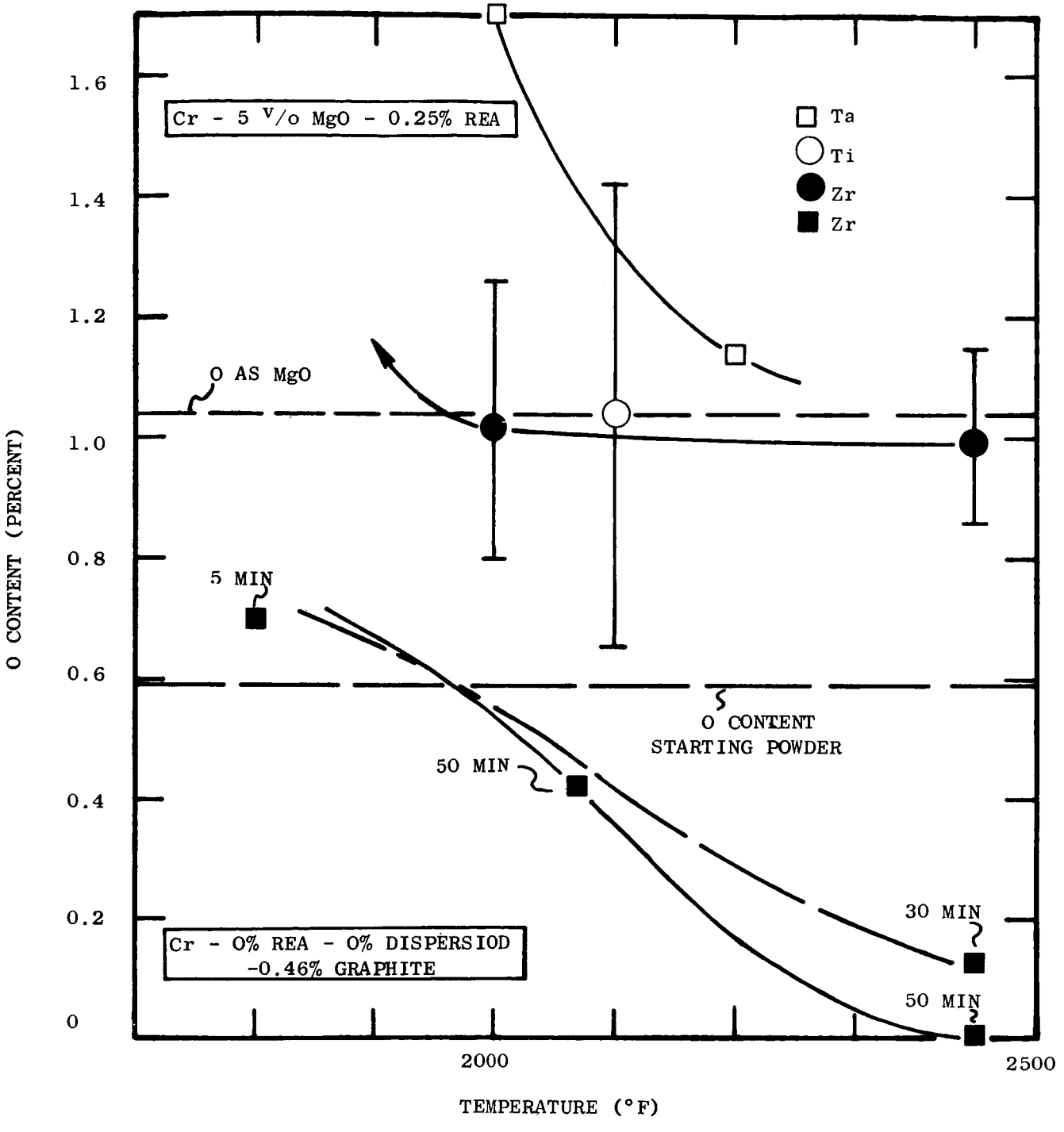

FIGURE 7 Reduction of O in Cr Powders during Carbothermic Cleaning At Various Temperatures.

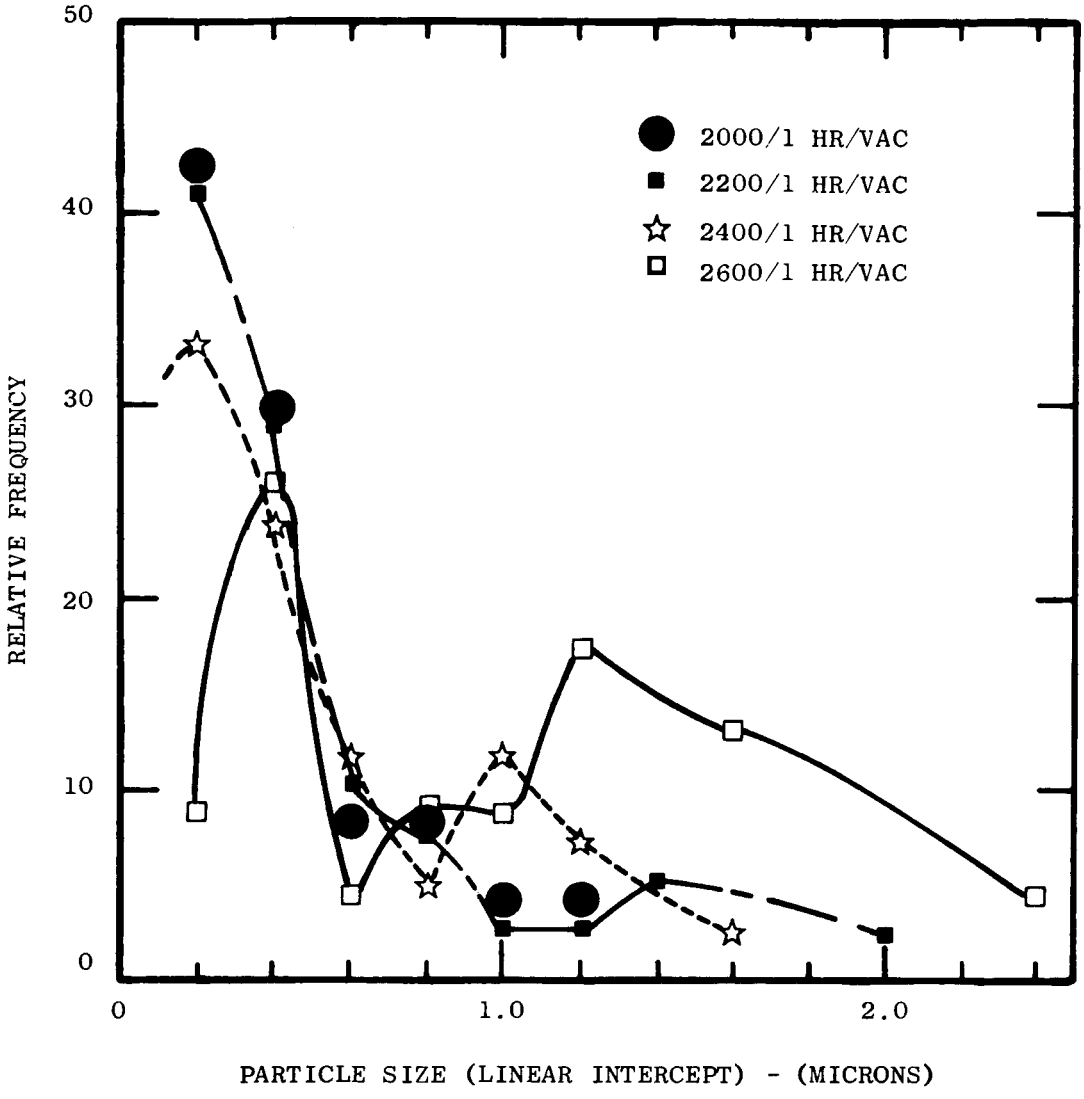

FIGURE 8 Frequency Distribution of MgO Particle Sizes in a Cr-5 ^{v}/o MgO-3.9% Mo-0.25 each Hf, Th, Y Compact as a Function of One Hour Vacuum Annealing Temperature.

(a)

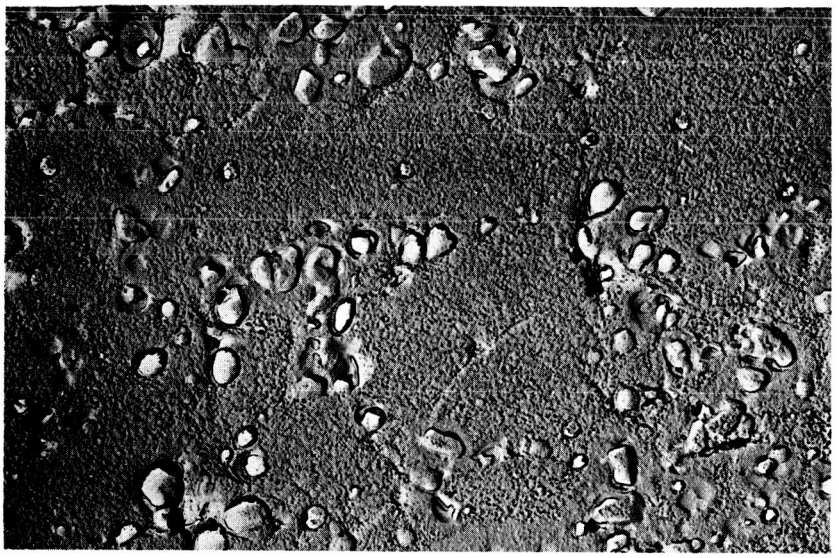

10,000X 666E

(b)

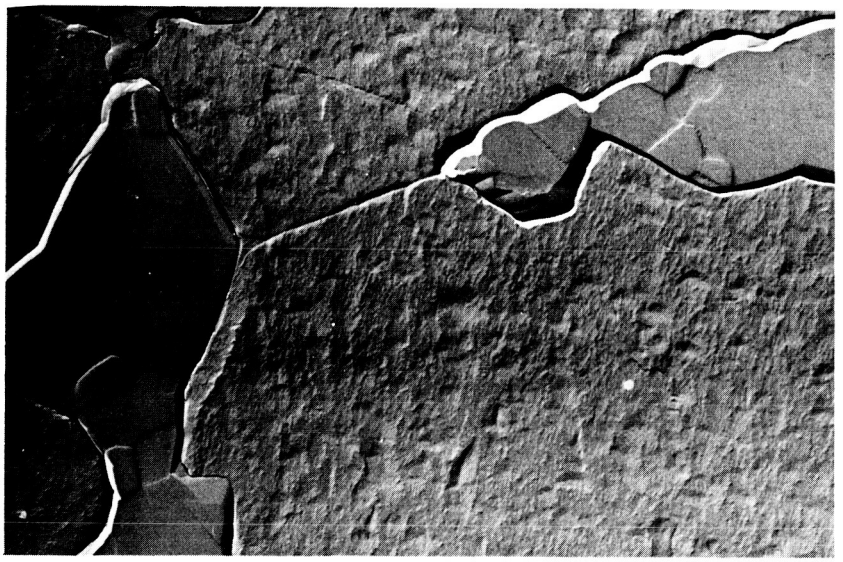

5000X 680B

FIGURE 9 Thermal Stability of Cr-5 $^{V}/_{o}$ Y_2O_3-.9 Mo-.15 ea Hf, Y, Th Alloy after Carbothermic Cleaning at 2200°F/20 min/Zr (60 ppm C, 0.83% Excess O_2). (a) As Autoclaved. (b) Autoclaved + Extruded + 2400°F/10 hrs Thermal Exposure.

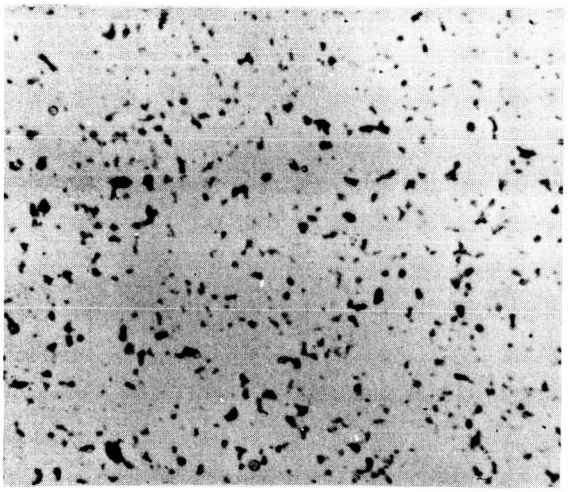

M1280

(a) 2000°F/5 min/Ta boat

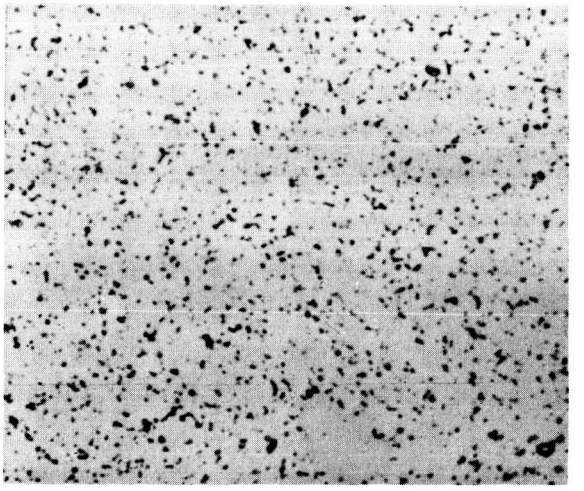

M1282

(b) 2200°F/5 min/Ta boat

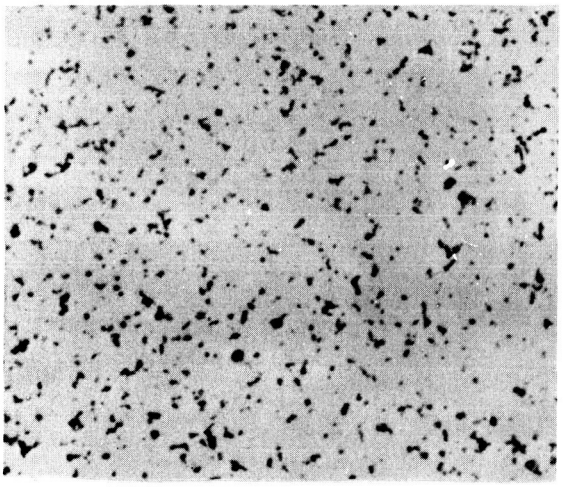

M1284

(c) 2400°F/5 min/Ta boat

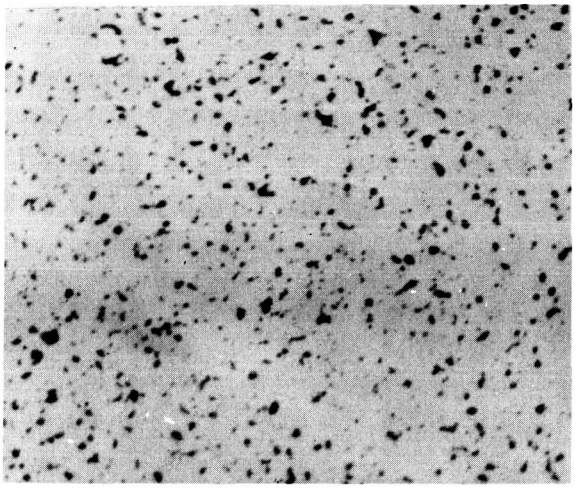

M1290

(d) 2000°F/50 min/Zr boat

FIGURE 10 M&R Cr-5 ^{v}/o MgO-1.0 Mo-.25 ea Hf,Th,Y Alloys after Carbothermic Cleaning According to Conditions Shown. All Samples were Densified by Autoclaving at 2000°F for Two Hours at 10 ksi.

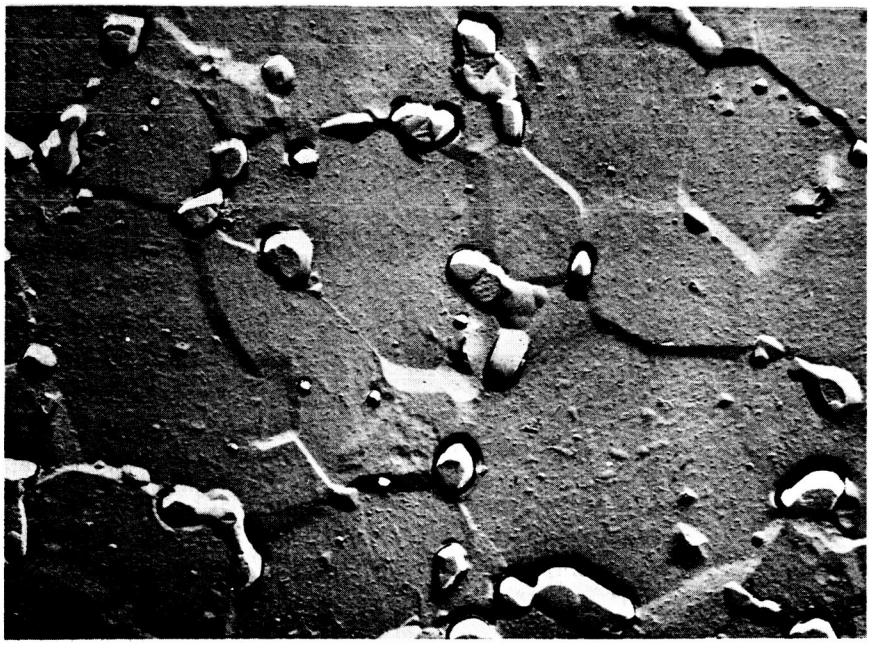

10,000X 638A

(a) 2200°F/5 min/Ta boat

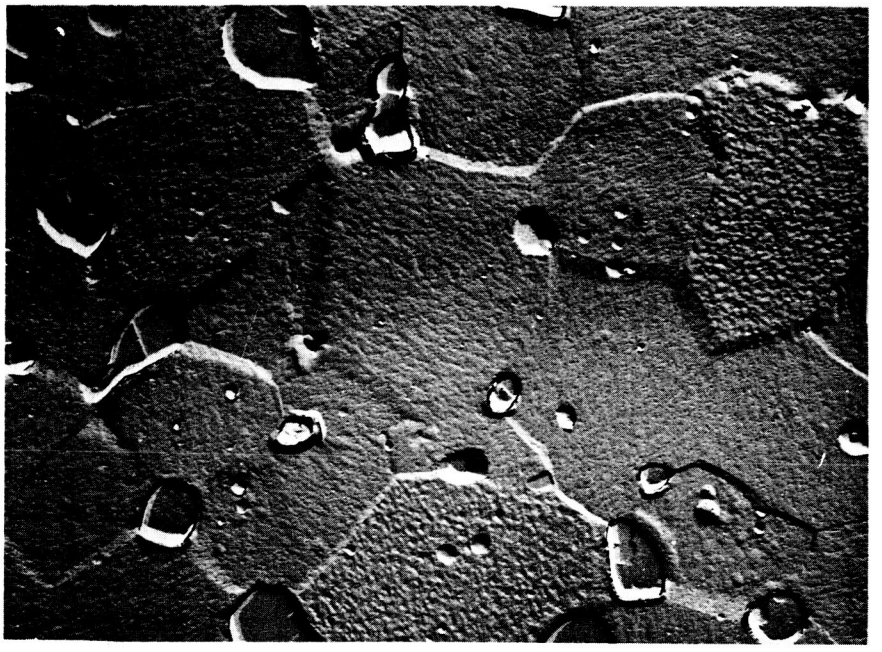

10,000X 638B

(b) 2000°F/50 min/Zr boat

FIGURE 11 Electron Photomicrographs of Cr-5 ^{v}/o MgO, 1.0 Mo-.25 ea Y, Th, Hf Alloy Shown in Figure 10 (b and d). Germanium Shadowed Two Stage Carbon Replica.

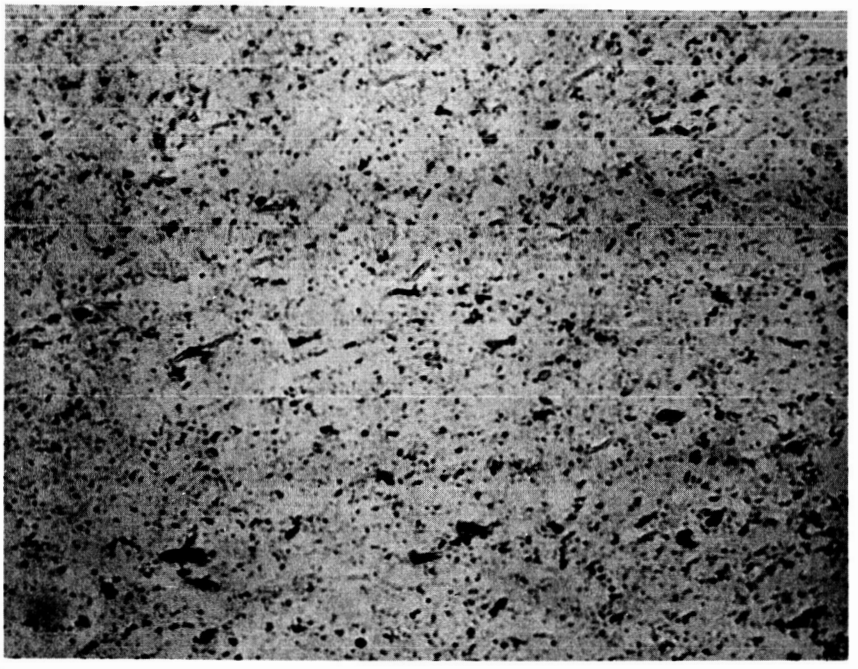

(a)

1000X

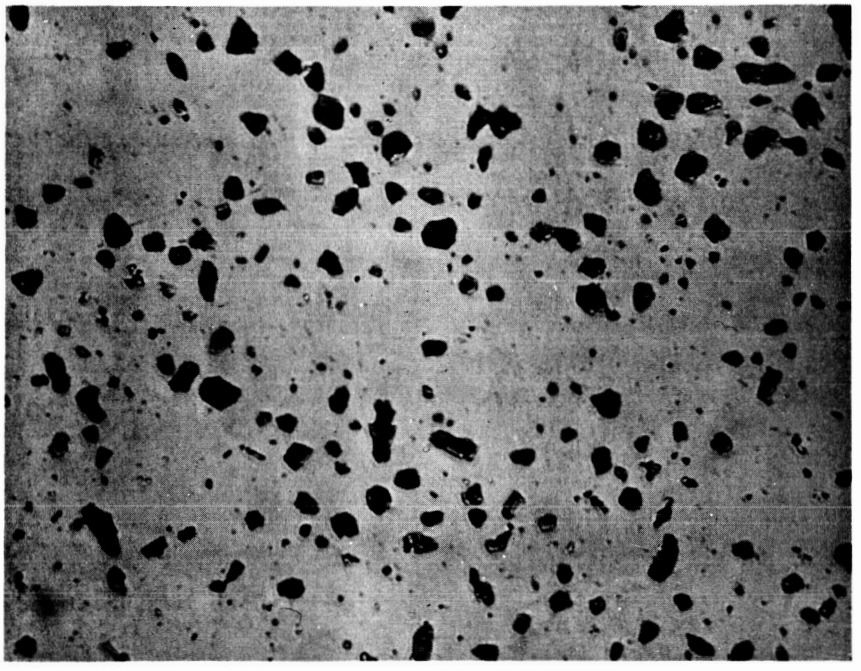

(b)

1000X

FIGURE 12 Dispersoid Stability of Cr-5 $^{V}/o$ Y_2O_3-3.45% Mo-0% REA Alloy Containing 60 ppm C and 1.3% Excess Oxygen. (a) As-Compacted. (b) As-Compacted + 2600°F/1 hr/vac.

(a)

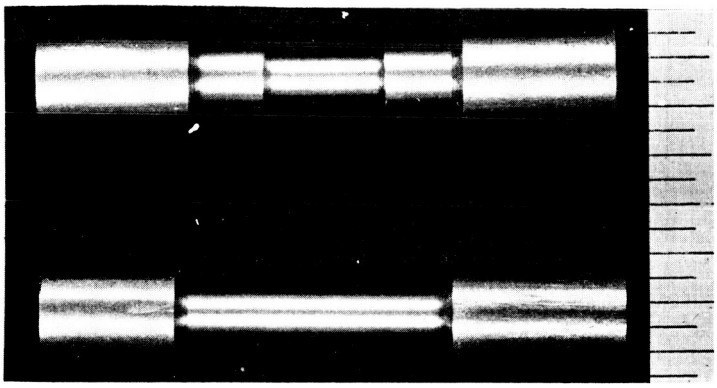

2X C66061601

(b)

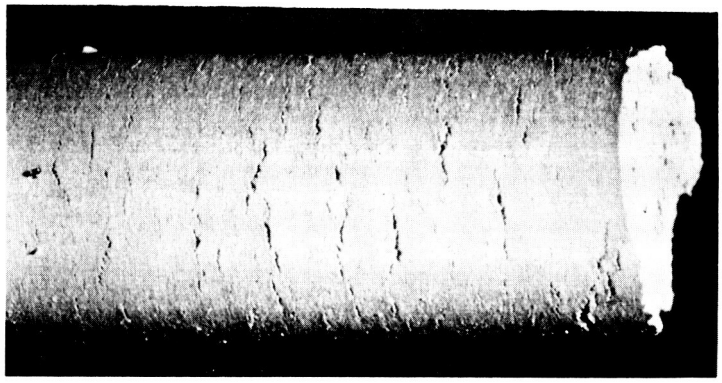

10X C66062802

(c)

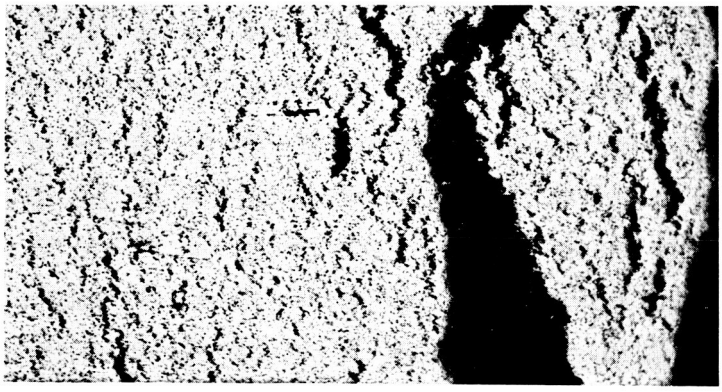

100X M4247

FIGURE 13 Cr-5 $^{v}/_{o}$ Y_2O_3-.9 Mo-.15 REA Tensile Specimen: (a) Original Specimen Configuration for DBTT (top), and Tensile Testing (bottom); (b) Macrophotograph of 2000°F/vac Tensile Fracture; (c) Longitudinal Microstructure of Fracture Gage Length Shown in (b).

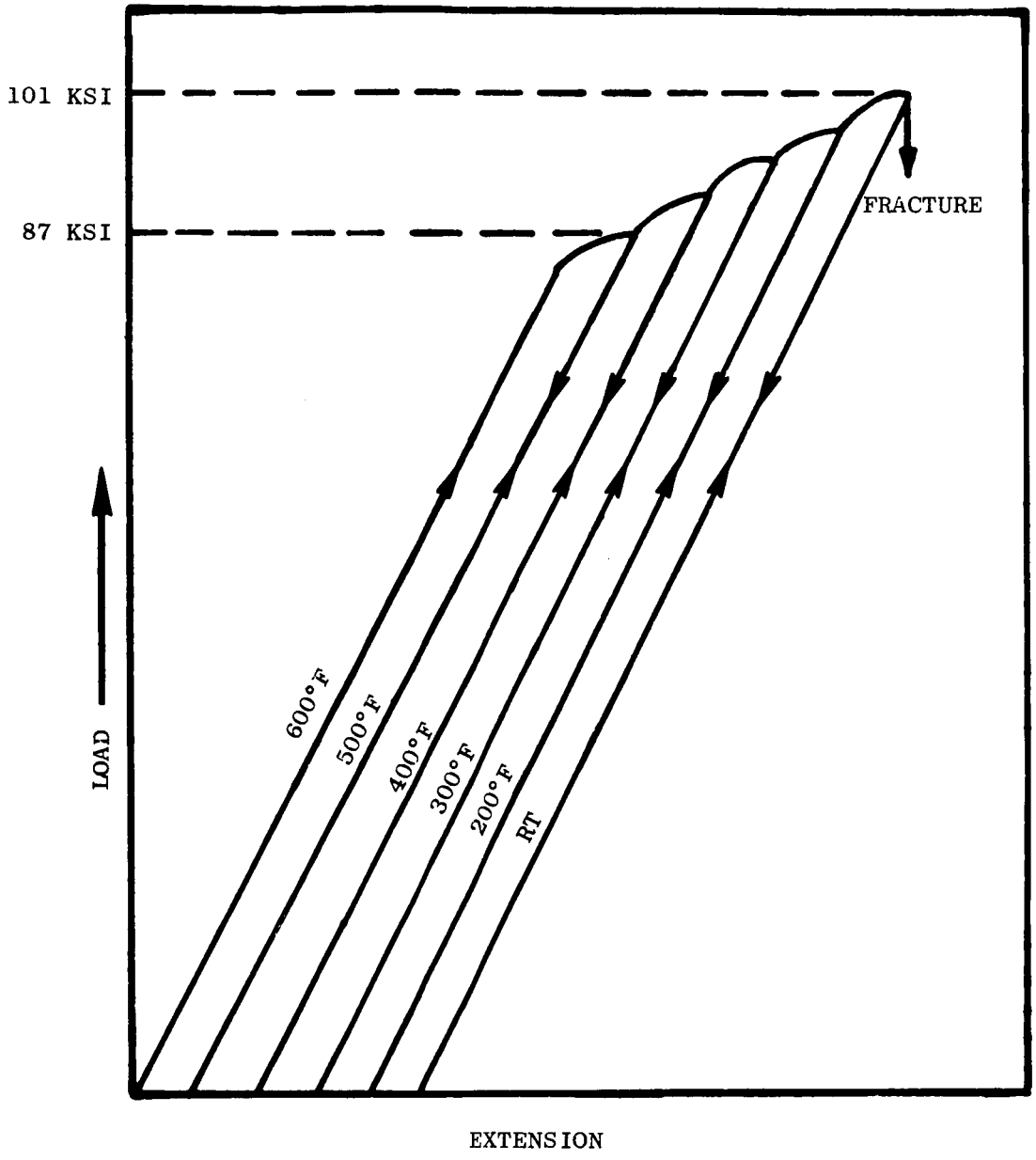

FIGURE 14 Instron Chart Tracings Showing Load Versus Extension (Time) For the DBTT of Cr-5 $^{V}/_{o}$ Y_2O_3-1Mo-0.15 Hf, Th, Y. Each Extension Cycle Corresponds to 1% ε.